stellarator news

Published by Fusion Energy Division, Oak Ridge National Laboratory
Building 5700 P.O. Box 2008 Oak Ridge, TN 37831-6169, USA

Editor: James A. Rome Issue 92 May 2004
E-Mail: jar@ornl.gov Phone (865) 482-5643
On the Web at *http://www.ornl.gov/sci/fed/stelnews*

First components of Wendelstein 7-X ready for assembly

The first major components for the Wendelstein 7-X (W7-X) experiment have been delivered to the Greifswald branch of Max-Planck-Institut für Plasmaphysik (IPP) to prepare for the assembly process that is scheduled to start this fall. Two magnet coils, the first plasma vessel segments, and vessel ports for the cryostat are now on site. Tests for the complex assembly procedure began in March (Fig. 1). The start of W7-X operation, scheduled for 2010, depends upon on-time completion of components by industrial suppliers.

Fig. 1. Test assembly at Greifswald: A coil-handling unit stringing a nonplanar coil with a weight of 6 tons across a 3-D shaped sector of the plasma vessel (Photo: B. Kemnitz).

The stellarator magnetic field of W7-X is produced by a total of 50 nonplanar coils resulting in a low-shear configuration with an edge rotational transform $\iota(a) = 1.0$, central $\iota(0) = 0.86$ at a minor radius $a = 52$ cm in the so-called standard case. The 20 auxiliary planar coils allow for variation of ι and application of a vertical magnetic field. Due to periodicity and stellarator symmetry only seven different types of coils — five non-planar and two planar — are necessary to realize the magnetic field configuration. Together, the seven coil types form the magnet system of one of the ten half-modules. In addition to these main coils, ten smaller control coils, one per half-module, introduce a $5/m$ field perturbation, thus modifying the plasma

In this issue . . .

edge configuration, which is used to adjust the properties of the island divertor.

The superconducting cable made of NbTi with a case of aluminium alloy was specially developed for W7-X. In operation, cooling to superconducting conditions is performed by liquid helium flowing inside the conductor. A total of 60 km of cable is required, more than 80% of which has already been produced by the supplier, a consortium of European Advanced Superconductors (Hanau, Germany) and Europa Metalli Superconductors (Italy). This conductor is being processed into winding packages by the consortium of Babcock Noell Nuclear and Ansaldo at ABB in Augsburg, Germany, and Ansaldo in Genova, Italy. Four of the approximately 3.5-m-high, 2.5-m-wide coils are ready; more than half of all the coils are being processed. The repetition accuracy of the winding packages within one type of coils meets the requirement of ±3 mm in most cases.

The conductor and also the entire winding pack are electrically insulated by fiberglass bandages and impregnated with epoxy resin for rigidity. To withstand the large Lorentz forces, these winding packs are embedded into solid steel casings (manufactured as half-shells by the Swedish foundry, Österby Gjuteri AB) at Babcock Noell Magnettechnik GmbH in Zeitz, Germany. Filling the space between the winding package and the steel casing with quartz sand and epoxy resin ensures uniform transmission of forces. During the cooldown to low temperatures, the casing and winding packages contract differently; the corresponding stresses are compensated by heating of the casing prior to impregnation. In this way, stresses in the coils are minimized at the low operating temperature. Each coil is tested to its design current at low temperature at a test rig at CEA in Saclay, France. IPP has now received the first two of the nonplanar coils at Greifswald.

The 20 planar superconducting coils are being manufactured at Tesla in the United Kingdom, where 16 coils have meanwhile been wound and 3 have been completed (Fig. 2). Three planar coils have also passed their performance test at Saclay

Fig. 2. One of the 20 planar coils during production at Tesla (Photo: Udo Arensmann).

The first 2 of a total of 20 segments of the plasma vessel (Fig. 3) were delivered to Greifswald by the manufacturer, MAN DWE (Germany) at the end of last year. Meanwhile, first magnetic diagnostics have been mounted onto the vessel walls. The next segments will follow at the end of April; from then on, a couple of segments are expected every second month. All coils are in the same toroidally shaped cryostat, which is composed of two shells. The outer one is the so-called vacuum vessel, which houses everything. The inner shell is the so-called plasma vessel enclosing the volume for the plasma and in-vessel components. In between these two vessels are the coils. Ports cross the vacuum space between these two shells and give access to the plasma vessel interior. A major challenge of the plasma vessel design was to optimize the shape in order to give maximum space for the plasma while keeping the necessary clearance against the cold coils. As a consequence, the tolerances for the plasma vessel shape had to be reduced to ±3 mm. The required shape is reproduced by assembling the vessel from 200 individual stainless steel rings. Each ring is made up of several sheet metal strips, with a thickness of 17 mm and a width of 15 cm, which are multiply creased to reproduce the curved contours. Finally, apertures for the ports are cut by high-pressure water jets.

The outer vessel of the cryostat, with a major diameter of 16 m and a minor diameter of 4.5 m, is also being manufactured by MAN DWE and will be delivered as half-shells for each module. The first half-shell is scheduled for mid-2005, in time for its on-site assembly preparation. For cooling of the magnets and their support structure — a total mass of 425 tonnes — a helium refrigeration plant will be delivered by Linde Kryotechnik (Switzerland) in 2007. The plant will supply an equivalent power of 5000 W of helium refrigeration to a temperature of 3.4 K.

Fig. 3. One of 20 segments of the plasma vessel for Wendelstein 7-X. Apertures for port access and cooling pipes located at the outboard side can be seen (Photo: W. Filser, IPP).

Access to the plasma vessel is given by 299 apertures in the vessel segments, many of them required for the handling of high-power steady-state operation, which is a final goal of the W7-X project. Corresponding ports connect the plasma vessel with the outer vessel by using the spacing between the coils. These ports are dedicated for diagnostics and cooling of first wall and in-vessel components (140 ports), operation and infrastructure of the divertor (120 ports), plasma heating (19 ports), and pumping (20 ports). All ports are equipped with flexible bellows to compensate for changes in length during bakeout of the plasma vessel. Port dimensions range from a diameter of 100 mm to apertures of 400×1000 mm^2 with a typical length of 1.5 m. Meanwhile 60 ports of the first module, manufactured by the Swiss company Romabau, have been delivered (Fig. 4).

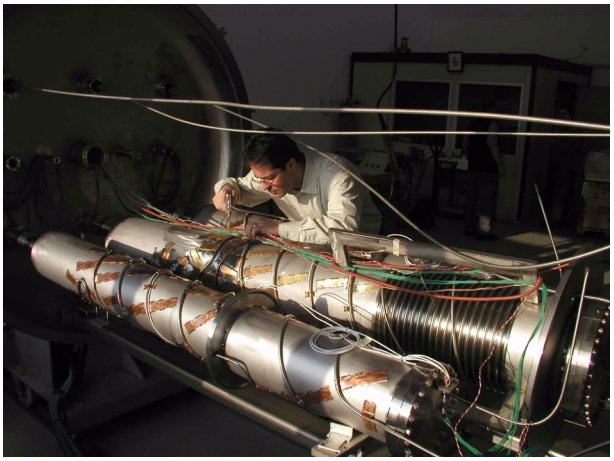

Fig. 4. Two ports during their vacuum test at the supplier Romabau (Photo: B. Sombach).

With all of these components on site at Greifswald, first tests of the assembly sequence are now being performed (see Fig. 1).

Isabella Milch and Matthias Hirsch for the W7-X project
Max-Planck-Institut für Plasmaphysik
Division E5
Teilinstitut Greifswald
Wendelsteinstraße 1
D-17491 Greifswald
Germany

E-mail: matthias.hirsch@ipp.mpg.de

Phone: +49-3834-88-2536
FAX: +49-3834-88-2009

Neutral beam injection at TJ-II

Introduction

The first neutral beam injection (NBI) plasmas in TJ-II were obtained in the most recent experimental campaign. The neutral H^0 beams had an energy of 28 keV, port-through power between 200 and 300 kW, and pulse length between 100 and 200 ms. The aims of the campaign were to get started with NBI operation, test and tune up the special control features required for NBI, adjust diagnostics to the new environment, and study beam-plasma coupling under different scenarios [different TJ-II magnetic configurations, different gas puffing/electron cyclotron heating (ECH) timing strategies, etc.].

Neutral beam injection at TJ-II

The NBI system at TJ-II consists of two tangential injectors in a co-counter configuration. The injectors and ion sources are a loan from Oak Ridge National Laboratory, through a collaboration contract with the U.S. Department of Energy. Auxiliary systems such as high voltage power supplies, water cooling system, primary vacuum system, and control and data acquisition systems have been provided by the Fusion Laboratory at CIEMAT in Madrid, Spain.

Beam simulation studies have shown that with the ion source operated at nominal parameters, the injected beam should reach 0.9 MW. The low beam transmission (62% of the neutralized beam) is due to the high beam divergence (1.3º) and the narrow aperture through the duct and past toroidal field coil TF1. In order to protect TF1, it was necessary to install a beam diaphragm in the duct that accounts for the greatest part of the geometrical losses. Because the beam simulation studies were made early in the project development, some measures to forestall the high reionization losses associated with an increase of pressure in the duct due to thermal desorption. Therefore, two extra titanium getter pumps were installed in the calorimeter box, very near the beam diaphragm.

Injector 1 is fully commissioned and operative. We have obtained beams of 30 keV and 50 A at the ion source. To proceed with ion source conditioning up to the nominal values (accelerator voltage of 40 kV and current of 100 A), the high-voltage power supplies need further improvements (tetrodes must be replaced).

Injector 2 is presently undergoing installation. The auxiliary systems were provided in parallel with those of injector 1, so they are already in place. But some mechanical pieces need modifications and repair, as was made clear during first vacuum tests last December. We expect to start conditioning for this source at the end of this year.

First results of NBI heated plasmas

The target plasma for the neutral beams is heated with ECH, using one or two 53.2 GHz, 250-kW gyrotrons.

A common feature of the NBI plasmas is that after a slow initial increase in density, the attainment of ECH cutoff is followed by a rapid density increase that continues to the end of the discharge or to plasma collapse before the scheduled termination time. Soft X-ray signals show a sudden cooldown of the electrons at cutoff, normally followed by a temperature stabilization and subsequent increase, as shown in Fig. 1.

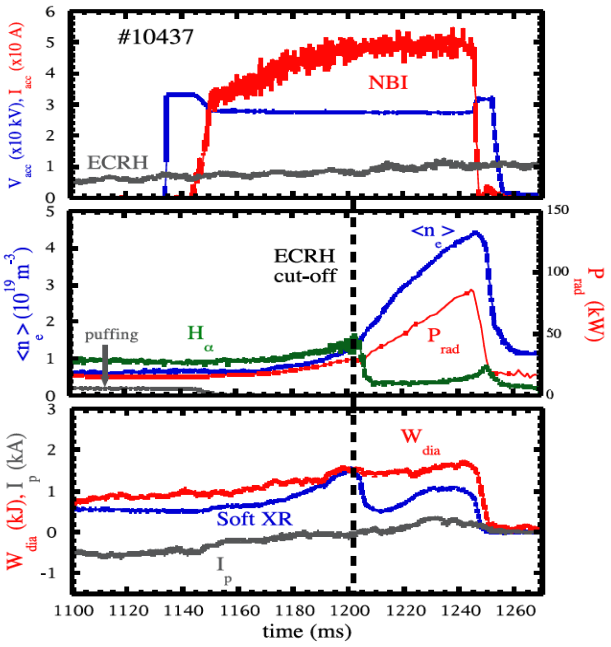

Fig. 1. NBI and ECH parameters (top) for a typical TJ-II discharge. The density rises sharply after ECH cutoff (center), but the soft X rays drop, indicating a cooldown of the electrons (bottom).

The transition from ECH to NBI plasmas is characterized through the different diagnostics. Thomson scattering profiles show a transition from the typically hollow density profiles (central value of 1.7×10^{19} m^{-3}) of ECH plasmas to peaked, broad profiles (central value of $4–5 \times 10^{19}$ m^{-3}) after NBI sets in. Electron temperature profiles evolve from the center-peaked, narrow shape of ECH plasmas to the broader, lower peak value (200–300 eV) of the NBI case.

Plasma edge density as measured by lithium thermal beams shows a consistent behavior at the transition from ECH to NBI regimes: the density tails usually observed in the scrape-off layer (SOL) region ($\rho > 1.0$) in ECH plasmas disappear in the NBI phase.

There is a simultaneous reduction in the radial $\boldsymbol{E}\times\boldsymbol{B}$ turbulent particle flux measured with Langmuir probes and in the particle recycling as reflected by the H_α signal. All of these features seem to point toward an improved confinement regime. Several MHD modes below 300 kHz have been found in the frequency spectra of magnetic pickup coils in the NBI regime.

The observed collapse of the discharge does not seem to be related to an increase in Z_{eff}. Vacuum ultraviolet spectra taken before and after the onset of NBI show that there is no significant increase of metals (Fe, Cr) or light impurities (B, C, O, F) during the NBI pulse. Recent experiments have identified an increase of edge transport near the TJ-II density limit, from the edge up to far into the SOL region. These results suggest the importance of both radiative and edge transport mechanisms in the physics of the density limit in the TJ-II stellarator.

Beam simulation and transport studies

Neutral beam absorption studies have been performed by means of a Monte Carlo computer code. Measured plasma temperature and density profiles are introduced in the code, which then calculates the different beam loss ratios and the absorption profiles for ions and electrons. The results show that for a beam of 28 keV, 42 A at the ion source, 75% of the power is absorbed by the plasma at densities near 4×10^{19} m^{-3}. Particle fueling cannot account for the increase in plasma density; other mechanisms, such as an improved confinement and wall influx, must be invoked.

The transport code PROCTR has been used to calculate ion temperature profiles and the electric field distribution. Data input included the power density profiles from the neutral beam absorption calculation and the radiated power profile. The resulting ion temperature profiles correspond to a thermal equilibrium between ions and electrons, with central temperatures near 300 eV. The calculated electric field is negative at all radii inside the plasma, having a maximum absolute value at $\rho = 0.6$, where the measured plasma density profile has the maximum gradient.

Conclusions

- First, low-power neutral beams (28 kV, 200–300 kW) have been injected into TJ-II.
- Density control has not been achieved so far. The density increases dramatically, often leading to a discharge collapse.
- At the plasma edge, the sharp decrease of turbulent transport and the change in the density profiles hint at an improved confinement mode.
- Impurities do not seem to be a problem; Z_{eff} remains low (<1.5).
- Typical NBI plasma features are seen: broadened profiles, plasma rotation, plasma potential, and MHD instabilities.
- Maximum achieved densities are compatible with the stellarator density limit.

Macarena Liniers on behalf of TJ-II Team
Laboratorio Nacional de Fusion
Asociación EURATOM-CIEMAT
Av. Complutense 22
28040 Madrid, Spain

E-mail: macarena.liniers@ciemat.es

References

[1] M. Liniers, J. Alonso, et al., "Neutral Beam Injection System for TJ-II," Proceedings of the 20th Symposium on Fusion Technology, Vol. 1, p. 307 (1998).

[2] J. Guasp, M. Liniers, C. Fuentes, and G. Barrera, "Thermal Load Calculations at TJ-II Vacuum Vessel Under NBI," Fusion Technol. **35**, 32–41 (1999).

[3] C. Alejaldre et al., "Overview of TJ-II experiments," presented at the 14th International Stellarator Workshop, Greifswald, Germany, 2003.

Confinement study based on an extended international stellarator database: An interim report

The configuration space of possible stellarator designs is quite large, so comparative studies of experimental behavior are important to making choices that lead to an attractive reactor. Both experimental and theoretical confinement studies have been intensively conducted in a variety of concepts for a long time. In the past decade, large experiments and findings of improved modes have advanced parameters, and theoretical and design studies have led to the development of advanced configurations for the next generation of experiments. We have started to revise the international stellarator database, incorporating these new data to improve the assessment of potential stellarator reactors and deepen thee understanding of the underlying physics of confinement. Here we make an interim report of progress. The database is jointly hosted by the National Institute for Fusion Science (NIFS) in Japan and the Max-Planck-Institut für Plasmaphysik (IPP) in Germany.

In 1995, a collaborative international study used available data from medium-sized stellarator experiments (i. e., W7-AS, ATF, CHS, and Heliotron-E) to derive the ISS95 scaling relation [1],

$$\tau_E^{ISS95} = 0.079 a^{2.21} R^{0.65} P^{-0.59} \bar{n}_e^{0.51} B^{0.83} \iota_{2/3}^{0.4}$$
$$\propto \tau_{Bohm} \rho^{*-0.71} \beta^{-0.16} \nu_b^{*-0.04} \quad (1)$$

Here confinement time τ_E is in seconds, power P is in megawatts, and line-averaged electron density $\bar{n}_e$ is in particles per cubic meter (10^{19} m^{-3}), $\iota_{2/3}$ is the rotational transform at $r/a = 2/3$; ρ^* is defined as the ion gyroradius normalized by the plasma minor radius, and ν_b^* is the collision frequency between electrons and ions normalized by the bounce frequency of particles in the toroidal ripple.

Since ISS95, several new experiments, (LHD [2], TJ-II [3], Heliotron J [4], and HSX [5]), most with different magnetic configurations, have started. One older device, W7-AS, has used divertor operation to obtain an improved confinement mode [6,7]. Extension of the confinement database aims at confirmation of our previous understanding of ISS95 and examination of possible new trends in the confinement performance of stellarators.

To date, data points representing 2681 discharges have been added to the confinement database. The largest device, LHD (R/a = 3.9 m/0.6 m) has extended the parameter regime to substantially lower ρ^* and ν_b^* regimes which are 3–10 times closer to the reactor regimes than those of the mid-size devices (Fig. 1). Data from the flexible heliac TJ-II allow us to investigate the ι dependence over a much larger variation ($1.3 < \iota < 2.2$) than is available in the other experiments.

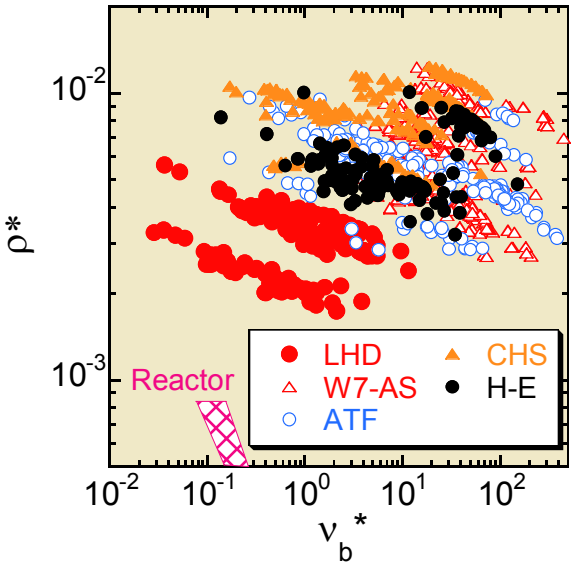

Fig. 1. Parameter regime of data in the international stellarator database in the space of normalized gyroradius ρ^* and collisionality ν_b^*.

A simple regression analysis of the entire data set using the same parameters as in ISS95 yields

$$\tau_E^{Reg} = 0.030 a^{2.07} R^{1.02} P^{-0.60} \bar{n}_e^{0.58} B^{1.08} \iota_{2/3}^{-0.16}$$
$$\propto \tau_{Bohm} \rho^{*-1.95} \beta^{0.14} \nu_b^{*-0.18} \quad (2)$$

with root-mean-square error (RMSE) = 0.101. If the data set consisted of an infinite number of independent, decorrelated data and the set of regression parameters were sufficient, this simple approach would be successful. This is not the case for our study, and application of Eq. (1) to data from a single device leads to contradictory results. Comparison of dimensionally similar discharges in LHD indicates that the transport lies between Bohm and gyro-Bohm scalings, while Eq. (2) is an unusually strong gyro-Bohm scaling. Rotational transform scans in TJ-II show a clear scaling $\tau_E \propto \iota^{0.5}$, which contradicts the weak dependence of Eq. (2).

We conclude that while Eq. (2) is useful for unified data description, its application is limited to the available data set alone and is not valid for extrapolation. Data inspection and experience from inter-machine studies suggest a need to introduce a magnetic-configuration-dependent parame-

ter in order to supplement the set of regression parameters and resolve this seemingly contradictory result.

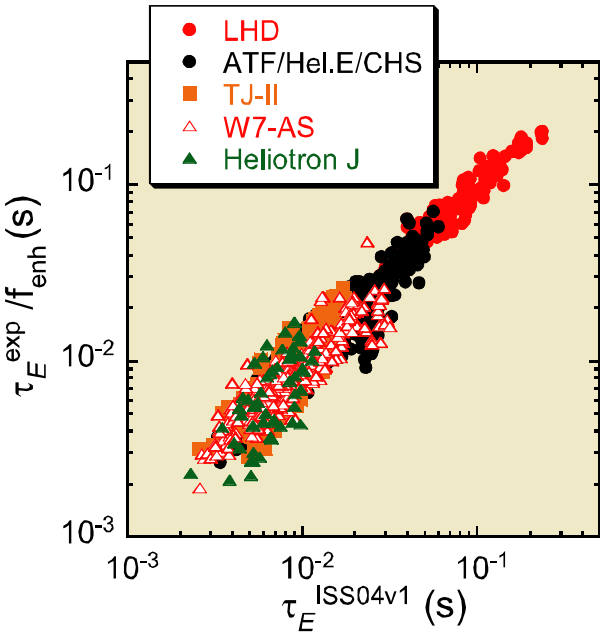

Fig. 2. Comparison of energy confinement in experiments and predicted by ISS04v1. Experimental data are corrected by an enhancement factor f_{enh}.

A systematic gap between W7-AS and heliotron/torsatron configurations was noted during the derivation of the ISS95 scaling. A recent example showing the pronounced effect of magnetic configuration variation even in a single device has come from comparison of the performance of configurations with shifted magnetic axes in LHD. A discharge with a strong inward shift of the magnetic axis, from R_{ax} = 3.9 m to R_{ax} = 3.6 m, results in a doubling of τ_E for similar operational parameters a, P, $\bar{n}_e$, B and ι [8]. Therefore, acceptance of a systematic difference in different magnetic configurations is a prerequisite for derivation of a useful unified scaling law. A deterministic parameter characterizing the magnetic configuration has not yet been discovered, but certainly involves the details of the helically corrugated magnetic fields, so an enhancement factor on ISS95 is used for description of the magnetic configuration effect. One enhancement factor is defined by the average value of experimental enhancement factors for each configuration. Iteration of a regression analysis of data normalized by these enhancement factors specific to configurations results in a new proposed scaling law, ISS04v1:

$$\tau_E^{ISS04v1} = 0.143 a^{2.33} R^{0.60} P^{-0.64} \bar{n}_e^{0.59} B^{0.89} \iota_{2/3}^{0.47}$$
$$\propto \tau_{Bohm} \rho^{*-1.15} \beta^{-0.16} \nu_b^{*0.02} \quad (3)$$

with RSME = 0.089 (see Fig. 2). This expression appears more comprehensive than Eq. (2). The leading coefficient is determined so as to give an enhancement factor of 1 for the case with $\iota < 0.48$ in W7-AS, and Fig. 3 shows the enhancement factor for different experimental devices.

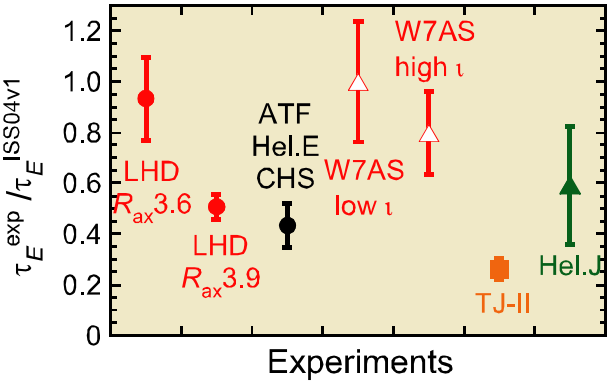

Fig. 3. Enhancement factors for devices considered. Data for W7-AS are divided into two groups with low ι (<0.48) and high ι (≥0.48).

These results lead to two tasks for the immediate future of these studies. The first is to refine the regression analyses of revised data in subgroups with variable parameters. The second, more challenging step is to determine the enhancement factors in terms of specific properties of the helical field structure of the devices. Then we will project the observed optimal confinement properties of the large W7-AS and LHD devices — which are comparable to the tokamak ELMy H-mode scaling [IPB98(y,2)] — to fusion parameter regimes to develop operational scenarios for currentless stellarator reactors.

The Web page of the international confinement stellarator database is available at both
http://iscdb.nifs.ac.jp/
and
http://www.ipp.mpg.de/ISS.

Acknowledgments

We are grateful to the LHD, W7-AS, TJ-II, Heliotron-J, and HSX experimental groups for their contributions to the international stellarator database. In particular, discussions and communications with Drs. C. Beidler, R. Brakel, V. Dose, K. Ida, Y. Igithkhanov, H. Maassberg, D. Mikkelsen, S. Murakami, R. Preuss, A. Weller, K. Yamazaki, and M. Yokoyama are appreciated. We also thank Dr. A. Kus for his technical assistance. The activity of the international stellarator database is organized under the auspices of IEA Implementing Agreement for Cooperation in Development of the Stellarator Concept.

H. Yamada,[1] J. H. Harris,[2] A. Dinklage,[3] E. Ascasibar,[4] F. Sano,[5] S. Okamura,[1] J. Talmadge,[6] U. Stroth[7]

1. National Institute for Fusion Science, Toki, Gifu 509-5292, Japan.
2. Australian National University, Canberra, Australia.
3. Max-Planck-Institut für Plasmaphysik, EURATOM Association, Greifswald, Germany.
4. CIEMAT, Madrid, Spain.
5. Institute of Advanced Energy, Kyoto University, Uji, Kyoto, Japan.
6. University of Wisconsin, Madison, Wisconsin, USA.
7. University of Kiel, Kiel, Germany.

E-mail: hyamada@lhd.nifs.ac.jp

References

[1] U. Stroth et al., Nucl. Fusion **36** (1996) 1063.

[2] H. Yamada et al., Plasma Phys. Control. Fusion **43** (2001) A55.

[3] C. Alejaldre et al., Plasma Phys. Control. Fusion **41** (1999) A539.

[4] T. Obiki et al., Nucl. Fusion **41** (2001) 833.

[5] F. S. B. Anderson et al., Fusion Technol. **27** (1995) 273.

[6] K. McCormick et al., Phys. Rev. Lett. **89** (2002) 015001.

[7] A. Weller et al., Plasma Phys. Control. Fusion **45** (2003) A285.

[8] H. Yamada et al., Nucl. Fusion **41** (2001) 901.

Extended abstracts

Pumping capability and particle balance in W7-X: A self-consistent 3-D study

To be presented at the 16th International Conference on Plasma Surface Interactions, (Proceedings to be published in the Journal of Nuclear Materials)

Considerable modeling efforts with the three-dimensional (3-D) EMC3-EIRENE plasma edge transport code have been started to simulate the particle balance for stationary divertor operation in the stellarator Wendelstein 7-X (W7-X) presently under construction in Greifswald. A heating power of 10 MW of neutral beam injection (NBI) will contribute an estimated refueling rate of 2×10^{21} s^{-1} for a duration of 10 s. Strong pellet refueling of the same order of magnitude will be needed to control the density profile for long-pulse electron cyclotron resonant heating (ECRH) operation. With possible additional contributions from the wall recycling above unity due to gradually increasing wall temperature, the pumping system will have to handle total external particle fluxes up to 10^{22} s^{-1}.

The establishment of a stationary particle balance crucially depends on the divertor pumping efficiency, which, for a given particle input, sets a lower limit to the plasma density at the separatrix. In the present study, the neutral gas is modeled self-consistently with the background plasma in the presence of absorbing cryopump units housed in the divertor chamber. The main chamber wall is assumed to be in saturated equilibrium.

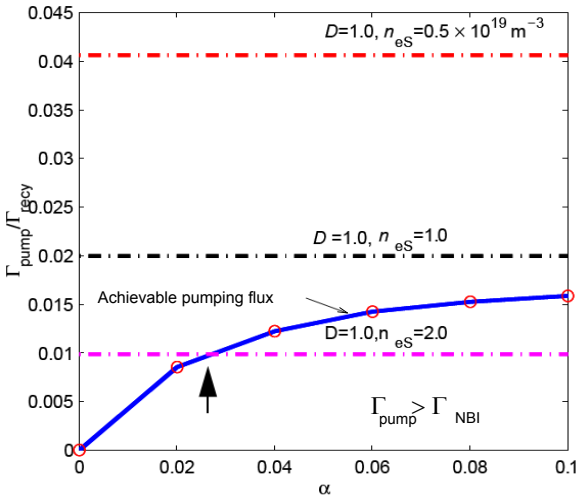

Fig. 1. The blue curve shows the dependence of the achievable pumping flux (normalized with the recycling flux) on the sticking coefficient of the active cryopump surface. The horizontal lines represent normalized fluxes that need to be pumped out at given separatrix densities considering a net particle input equivalent of 10 MW of NBI heating. The region under the blue curve represents the allowed parameter space for steady-state conditions.

For the W7-X standard configuration, with rotational transform $\iota = 5/5$, a cross-field diffusion coefficient of 1 $m^2 \cdot s^{-1}$, and total input power of 10 MW, the code simulations show that the normalized particle flux removable with the assumed geometry of the divertor and pumping system (blue curve in Fig. 1) lies within the range of 1 to 2% for sticking coefficients above 3%. This range corresponds to a minimum separatrix density between 1 and 2×10^{19} m^{-3}, which will be required to remove the specified NBI particle influx.

For lower densities, the removable particle flux would fall short of the fraction of recycling flux that needs to be pumped (straight lines in Fig. 1) in order to maintain a stationary condition. Improvement of the pumping efficiency by higher sticking coefficients is not expected because the achievable pumping flux quickly saturates, as shown in Fig. 1. This behavior was found to be true for the entire range of effective surface of the pumping gap area in the divertor design (Fig. 2). The rather low pumping efficiency predicted by the code is due to both the relatively open divertor geometry and the unfavorable position of the strike points with respect to the pumping gap in the standard configuration. An improvement of the local neutral compression, which is responsible for the neutral flux entering the divertor chamber, is possible by shifting the

strike point position closer to the divertor pumping gap and is presently being investigated.

The present study aims at optimization of the particle balance and pumping capability of W7-X at stationary conditions for the relevant ranges of magnetic configurations ($5/6 < \iota < 5/4$) and plasma parameters. Results will cover, in particular, estimates for the achievable pumping rate, pumping and recycling fluxes, divertor plasma, and neutral density distributions, as well as lower limits for separatrix density and required pumping area.

D. Sharma, Y. Feng, F. Sardei, J. Kisslinger, H. Grote, P. Grigull, and H. Renner
Max-Planck-Institut für Plasmaphysik
Teilinstitut Greifswald, Germany

E-mail: devendra@ipp.mpg.de

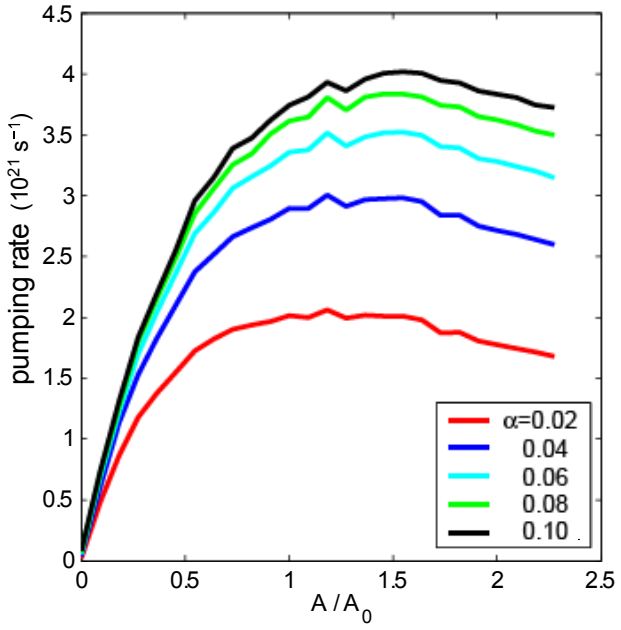

Fig. 2. The achievable pumping rate saturates with the sticking coefficient parameter α for all values of the effective pumping gap area A/A_0, where A_0 is the design value. Optimum pumping efficiency is found to be at the gap chosen in the current design, $A = A_0$.

Stationary and transient heat load in the island divertor of W7-AS

Plasma Phys. Control. Fusion **46** (2004) 711–721

Wendelstein 7-AS (W7-AS) is the first stellarator equipped with an island divertor where a 5/9 island chain that defines the plasma boundary is used for field line diversion to the ten divertor modules. The experiments also serve as a test for W7-X, since its modular island divertor and the edge structure will be similar to those of W7-AS. This paper reports the power load onto the divertor targets in W7-AS determined by means of infrared (IR) thermography, target calorimetry, and flush-mounted Langmuir probes.

For the stationary heat flux a reasonable agreement among the measurements by IR thermography and Langmuir probes is found. The heat fluxes obtained from thermography are systematically higher than those expected from calorimetry. This overestimation (up to 50% for specific tiles) is mainly attributed to inaccurate knowledge of specific tile geometries with respect to the IR picture. At a representative tile with high incident angle of the magnetic field lines, the stationary peak heat flux reaches 6 MW/m^2 at densities of 2.5×10^{20} m^{-3} with 2 MW of NBI. For lower densities, up to 8 MW/m^2 must be taken into account. The full width at half maximum (FWHM) of the divertor leg footprint is typically around 3–5 cm depending on the target and does not show a significant variation with heating power.

The temporal resolution of the IR thermography camera is 190 μs. For transient events, the uncertainty of the heat flux calculated from the surface temperatures measured with thermography can be a factor of two due to systematic errors resulting from the surface morphology. During edge-localized modes (ELMs) the measured peak heat flux reaches 25 MW/m^2 (see Figs. 1 and 2) for 2-MW NBI heating.

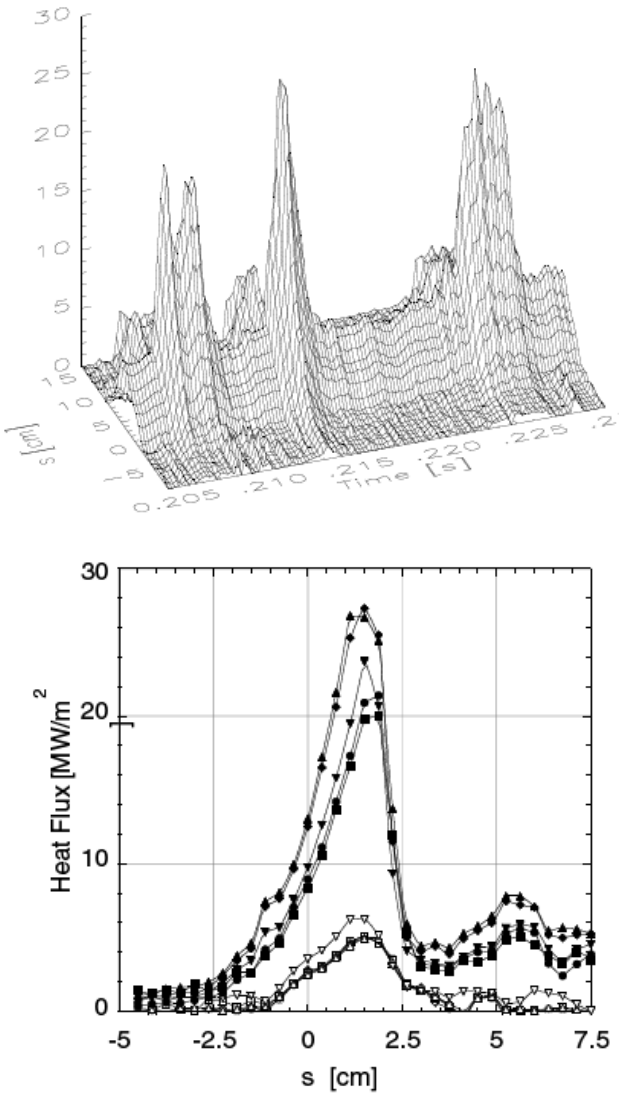

Fig. 1. Top: Heat flux deposition patterns measured at a tile with high incident angle of the magnetic field lines during a time interval of 25 ms in an ELMy H-mode. Bottom: Selected profiles during (full symbols) and between (open symbols) ELMs. The coordinate *s* points in radial direction.

This peak heat flux varies linearly with heating power. The power deposition profiles on the targets (measured with IR thermography at a time resolution of 190 μs and with target-mounted Langmuir probes with a resolution of 3 μs) show no significant broadening during an ELM if compared to the quiescent H-mode phases between the ELMs. From this we conclude that even during the ELM the ratio of parallel to perpendicular transport in the scrape-off layer remains constant, as reported also from type I ELMs in tokamaks. However, the relative intensity of the footprints for the different divertor legs (inner vs outer strike point and upper vs lower divertor) changes in the course of the ELM event by up to a factor of 4, as displayed by fast (3μs resolution) measurements with the arrays of target-mounted Langmuir probes.

F. Gadelmeier, A. Herrmann, D. Hildebrandt, K. McCormick, D. Naujoks, P. Grigull, M. Hirsch, and T. Klinger
Max-Plank-Institut für Plasmaphysik
EURATOM Association
D-17489 Greifswald, Germany

Contact: matthias.hirsch@ipp.mpg.de

Radiative condensation and detachment in Wendelstein 7-AS stellarator

Submitted to *Nuclear Fusion*

In the Wendelstein 7-AS stellarator under particularly high plasma density, a nonstationary radiation zone is observed to form on the inboard side of the torus. It causes a degradation of the diamagnetic energy of up to 50%. Configurational aspects of the magnetic field influence the development of the radiation zone as follows. The critical density is related to the connection length of the magnetic field; i.e., the observed degradation sets in at lower densities for magnetic configurations with large connection lengths (Fig. 1). Camera observation, in conjunction with forward calculations, indicates that the radiation zone is located on closed field lines and forms a toroidal belt. On the basis of complementary observations, it is concluded that the radiation zone is caused by a radiative condensation instability (or MARFE). Fluctuations of the radiation zone were recorded by a fast framing camera with a time resolution of 25 μs. Temporal variations as well as spatial movements are observed. The fluctuations are found on various lines of sight around the torus with correlation and phase shifts compatible with a toroidal propagation.

H. Thomsen, R. König, Y. Feng, P. Grigull, T. Klinger, K. McCormick, N. Ramasubramanian, U. Wenzel, and the W7-AS Team
Max-Planck-Institut für Plasmaphysik
EURATOM Association
D-17489 Greifswald, Germany

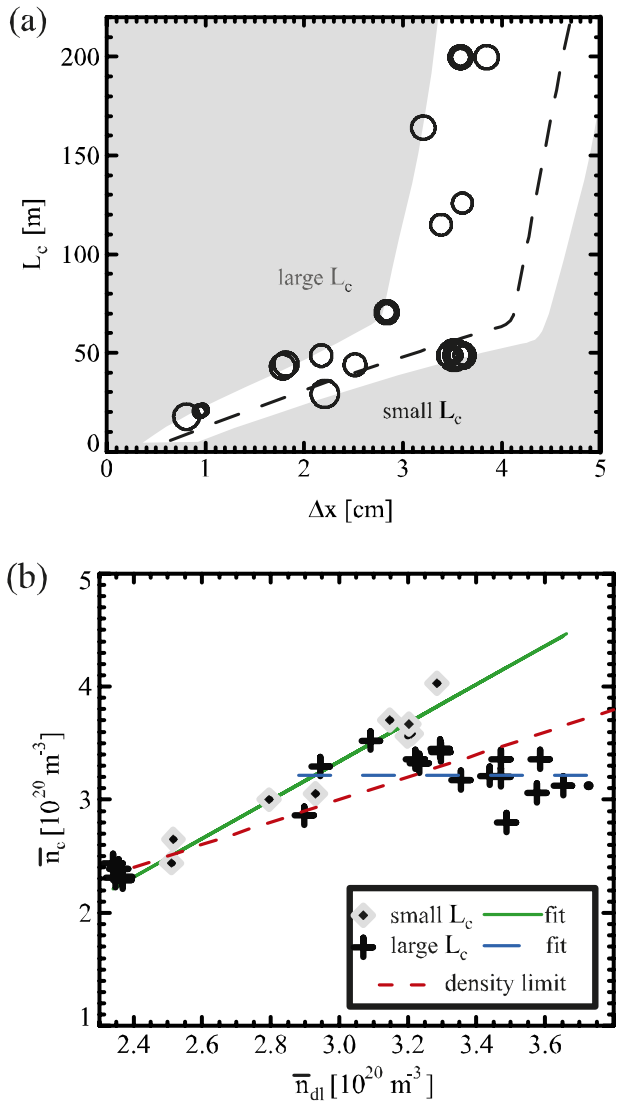

Fig. 1. (a) The divertor configuration discharges displaying a radiative degradation in the configurational space spanned by connection length L_c and island size Δx. The accessible region (limited by the control coil current) is shown in white. The discharges are sorted into two groups depending on their connection length (above and below the dashed line). (b) Critical density versus W7-AS density scaling. The line-averaged density just before the onset of the degradation is taken for each discharge. Crosses: discharges with large L_c. Diamonds:
discharges with small L_c. Solid lines: the respective fits. Red dashed line: density limit scaling.